

Spatio-Causal Patterns of Sample Growth

Andre F. Ribeiro*
ribeiro@alum.mit.edu

Abstract

Different statistical samples (e.g., from different locations) offer populations and learning systems observations with distinct statistical properties. Samples under (1) 'Unconfounded' growth preserve systems' ability to determine the independent effects of their individual variables on any outcome-of-interest (and lead, therefore, to fair and interpretable black-box predictions). Samples under (2) 'Externally-Valid' growth preserve their ability to make predictions that generalize across out-of-sample variation. The first promotes predictions that generalize over populations, the second over their shared exogenous factors. We illustrate these theoretic patterns in the full American census from 1840 to 1940, and samples ranging from the street-level all the way to the national. This reveals sample requirements for generalizability over space, and new connections among the Shapley value, U-Statistics (Unbiased Statistics), and Hyperbolic Geometry.

Keywords: Counterfactual Statistics, Spatial Statistics, Fairness, Generalization, Experimental-Design, Combinatorics.

*University of Sao Paulo, Sao Carlos, SP, 13560-970, Brazil.

1 Introduction

Large scale and high-dimensional geospatial datasets currently offer rich opportunities for predictive and Geo-AI [16, 27, 28] applications (e.g., disease incidence, ecological behavior, electoral results, crime occurrence, economic growth, recommendation systems), but little is known about how the generalizability and biasedness of Machine Learning and Artificial Intelligence models change, in practice, across space. Predictive algorithms are most commonly analyzed across bias-variance tradeoffs, using, for example, their out-of-sample accuracy ('predictiveness') and biasedness (black-box 'fairness') [5, 29]. We first formulate theoretic, closed-form functions describing fairness-generalizability tradeoffs across space (based in [23]), revealing their connections to hyperbolic geometry and experimental designs. We then consider 100 years of the American census (and all census variables) as case study. For each cross-section (decade), we consider the important task of predicting economic growth for over 60K individual locations with increasing spatial samples. We demonstrate how (1) generalizability tradeoffs evolve across spatial levels, and, (2) repeat the validation of generalizability limits derived in [23] for the spatial domain, and with the current census micro-data.

Let $S : X \rightarrow [0, 1]$ be any learning agent or system using input sample X^m with m variables, $S(X)$, to derive a classification decision. Our central goal is to formulate how the generalizability of these systems changes across space (i.e., to what extent a model assembled in a location will hold for others), and, thus, to identify a parametric functional form \mathcal{F} that can describe

$$\text{ACC}\left(S; X\left[x_0, d_{x_0}\right]\right) = \mathcal{F}\left(d_{x_0}\right), \quad (1)$$

where ACC indicates the accuracy of models, for any S , in samples $X[x_0; d_{x_0}]$ encompassing all observations at distances equal or lesser than d_{x_0} from x_0 . The **specific way in which \mathcal{F} changes across space offer limits and opportunities to agents and algorithmic learning and performance**. An increasing \mathcal{F} indicates that S are able to generate models that are accurate across locations, while a decreasing function indicate that learning fails to generalize across locations. A different issue is whether, from the same sample, S can identify the effect (or importance) of individual variables in the sample. These two problems reflect two key, but distinct, learning problems [15]: supervised out-of-sample prediction, and factor effect (or importance) estimation. Solutions to the former have become associated with the 'Machine Learning' moniker, and the latter with traditional causal effect estimation. More recently, the latter has also been studied when using, exclusively, the output of black-box supervised predictors [5]. The first stress the construction of predictive models, and the the second interpretable and unbiased models. We will demonstrate that combinatorial properties of samples impact these two traditional problems differently, and reveal tradeoffs across agents and locations.

The Shapley-value [24] has become an essential tool across disciplines to estimate the importance of variables from the output of black-box systems (i.e., whose inputs can be changed exhaustively at will) [18, 8, 5]. The value can be interpreted as the enumeration of all counterfactual effect observations in a **fully-observed** system [23]. This makes the Shapley value an instance of an U-Statistic and a permutation-based statistic [17, 11]. Both U-Statistics and the Shapley-value formulate relationships among sample statistic permutations and, respectively, their unbiasedness or 'fairness'. Calculating the **total number of permutations that can be enumerated in samples, or locations, thus sets strict bounds for their unbiasedness** [23], and offer a finer-grained illustration of these

relationships. While the relationship between the Shapley-value and fairness of black-box predictors is known [24, 18], their relation to generalization is perhaps more surprising [23]. A quantity that will therefore become central to formulate $\mathcal{F}(d_{x_0})$ theoretically, and trade-offs between the two previous learning problems, is the speed of growth, ω , in enumerable permutations across systems’ spatial levels, or their permutation ‘enumeration rate’.

2 A Combinatorial Perspective on Sample Growth

Statistical Sample Growth can be seen as the enumeration of populations, and their counterfactual observations. Let $X = \{a, b, c, \dots, [m]\}$ be a set of (observed or unobserved) binary factors¹ characterizing a population x , $x \in [0, 1]^m$, and $y(x)$ a measurement over the population, $y(x) \in \mathbb{R}$. Starting with a population x_0 , each possible sample growth trajectory (e.g., x_0, x_1, x_2, \dots) is an incremental, and temporally ordered, observation of the impact on y of gaining, or losing, a set of factors, from the m possible. In other words, each step in this trajectory is a counterfactual effect observation for x_0 , $\Delta y(x_0 - x_1) = y(x_0) - y(x_1)$ (where the former difference is over sets and the latter over scalars). A counterfactual effect observation is thus defined by: a difference in outcomes (the observed effect, $\Delta y(x_0 - x_1)$), a difference in factors (what changed, $x_0 - x_1$), and an intersection of factors (what remained the same, $x_0 \cap x_1$). For each trajectory and time, we can consider the biasedness and generalizability afforded by the accumulated samples to, for example, black-box predictors of y , and whether their performance is related to the increasing set of accumulated counterfactuals.

Counterfactual reasoning is central to Artificial Intelligence (AI). Counterfactual gain and loss predictions are central to the operation of most multi-agent and socio-economic

¹ $[m]$ is the m -th factor in sample X .

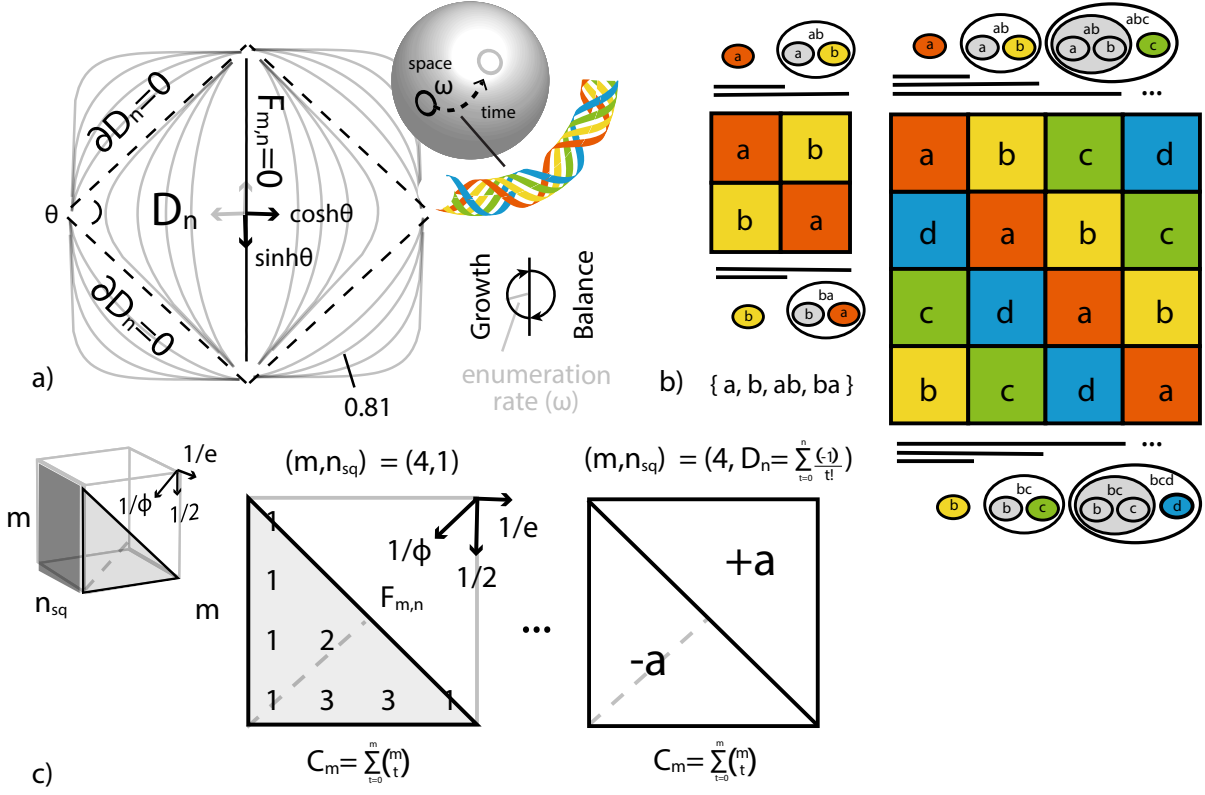


Figure 1: (a) Can counterfactual effect observations made in one location be used in another (are they externally valid, EV)? Can they be distinguished from others (are they unconfounded, CF)?, reciprocal growth and balance phases and their representation as hyperbolic rotations, (b) a $m \times m$ Latin-Square ('square') portrays the full set of counterfactual effect observations with m factors ($m = 2, 4$), more counterfactual observations increase guarantees over the generalizability and bias of samples' effect observations, (c) Binomial ($\frac{1}{2}$), Fibonacci ($\frac{1}{\phi}$), and Exponential ($\frac{1}{e}$) rates across squares lead to the hyperbolic relations in (a), each square's triangle (gray) altitude (dashed) is related to samples' permutation enumeration rate, ω .

systems (new products are counterfactuals over consumer preferences, hires over business labor forces, policies over societies, etc.) Most game-theoretic solutions, such as the Nash equilibrium, are formulated from counterfactuals (i.e., what would happen to a player’s utility if it took a given action, but all else remained constant). Understanding the statistical properties of counterfactual observations ex-post (i.e., their generalizability, biasedness), or sets of such observations, should therefore be central to the design and analysis of AI, multi-agent and learning systems.

Due to the causal interpretation (and associated results) offered by [23] (following from the traditional counterfactual approach to causal effect estimation [25]), we will say that samples undergo (1) Externally Valid (EV) growth when, throughout growth, back-box predictions remain general across exogeneous variation (and thus out-of-sample predictions remain accurate). They undergo (2) Unconfounded (CF) growth when effect estimates remain distinguishable (and thus predictions fair across sample populations). We expect black-box causal effect estimators to perform well in the second, and supervised out-of-sample predictors well in the first [23]. Understanding these alternative sample growth dimensions is important because they allow us to answer crucial questions for collected samples: Can predictions made in one location be used in another (are they externally valid, EV)? Can their independent effects be distinguished from other effects (are they unconfounded, CF)?

2.1 Combinations, Permutations and Partial Permutations

The set of all counterfactuals accumulated by sample growth at one instant can be visualized with a Latin-Square (‘square’), Fig.1(b). Squares are used here to highlight, and better visualize, the statistical properties of arbitrary sets of counterfactuals. A square, as defined

here, is a collection of all differences from a reference population x_0 , $x_0 - \mathcal{P}(X)$, where $\mathcal{P}(X)$ is the power-set (set of all subsets) of X . The square is thus associated with a full set of effect observations for any arbitrary measurement y . This is illustrated for two factors, $\{a, b\}$, in Fig.1(b, left). For a fixed sample X and reference x_0 , each counterfactual observation is defined by factor differences and intersections from x_0 . This suggests a map, or placement, of all sample units across square cells, for x_0 , with repetition. Every pair with a singleton difference from x_0 (and $m - 1$ overlapping factors) is associated with the square first column (and the individual difference, indicated by a Latin letter, with a row). A pair with two factor differences from x_0 , and with overlap from the first as indicated in its precedent first column, is associated with the second column, and so on. Fig.1(b, left) illustrates these combinatorial patterns with Venn diagrams for each cell when $m = 2$, where a cell's pairwise intersecting factors are grey.

When $X = \{a, b\}$, the simultaneous presence of populations $x_0 + \{a\}$, $x_0 + \{b\}$ and $x_0 + \{a, b\}$ (e.g., in the same location) allow for all permutations of $\{a, b\}$ be enumerated, and therefore each individual factor effect, $\Delta y(a)$ and $\Delta y(b)$, be observed, across full variation of others. When $X = \{a, b, c, d\}$, the square with $m = 2$ is associated with measurements robust to the variation in factors a and b , but susceptible to confounding (i.e., extraneous, or uncontrolled) variation of other factors (c and d) - unlike the $m = 4$ square, Fig.1(b, right). More abstractly, squares represent permutation groups [23], and each individual square is related to an U-Statistics for homogeneous populations [30]. The relationship of sample permutations to measurements' unbiasedness is a cornerstone of the most widely-accepted Theory of Non-parametric Statistics, U-Statistics [17, 11]. The relationship to generalizability has been discussed in [23], and is reviewed, and expanded, bellow.

The statistical concept of a 'population' is often associated with combinatorial com-

binations, as a set of units with a given attribute combination (e.g., high-income white males). There are thus $\binom{m}{t} = \frac{m!}{t!(m-t)!}$ populations of size t . A problem with this definition is that it leaves unspecified all non-population factors. To **define a population we imagine, instead, that we fix the t population factors and vary (i.e., 'permute') all non-population (i.e., 'external') factors.** This leads to a combinatorial structure known as a partial permutation. The number of partial permutations for a population of size t is $\binom{m}{t} \times D_{m-t}$, where D_{m-t} is the number of *derangements*² (permutations without overlaps). The full set of permutations, and all growth trajectories, can be formulated as sets of partial permutations,

$$m! = \sum_{t=0}^m \binom{m}{t} \times D_{m-t} \quad (2)$$

$$= \left[\cosh(m-1) + \sinh(m-1) \right] \times (m-1)! + 1. \quad (3)$$

The term $C_m = \sum_{t=0}^m \binom{m}{t}$ in Eq.(2) (a well-known factorial definition) corresponds to a single square [23] (i.e., one set of all differences), and Eq.(2) to all squares. The number of permutations in a sample can thus be specified succinctly by the 2D vector (m, n) , Fig.1(c, left), where $0 < n \leq D_{m-t}$. The odd and even parts of Taylor's expansion of Eq.(2) leads to hyperbolic trigonometric functions, Eq.(3) (proof in the *Supplementary Material*). They indicate the 'period' in which full sets of permutations are collected. We will refer to the (reciprocal of this) quantity as a sample's enumeration rate, ω , as it is associated with the number of permutations enumerated across time or spatial scales in systems. This quantity will be essential to understanding statistical tradeoffs across samples.

From a know interpretation of hyperbolyc functions [3], we demonstrate that sample

² $D_{m-t} = \sum_{k=0}^{m-t} \frac{(-1)^k}{k!}$.

growth can be decomposed in per capita growth and balance³ phases for the populations in a sample. Together, these cycles maintain basic statistical guarantees across *any* statistic derived from counterfactual observations - such as black-box and bootstrapping statistics fairness. Growth and balance are in many ways opposites, as growth bias balanced samples. A sample can grow monotonically across a single selected dimension, and that dimension is only guaranteed to be balanced once. Sample growth with balance can be understood, combinatorically, in relation to experimental designs and, geometrically, to hyperbolic geometry.

2.2 Sample Externally-Valid (EV) Growth

A singleton population $\{a\}$, defined as in the previous section (i.e., under high external variation), is represented by a square diagonal, Fig.1(b). Behind each square (and Shapley-value calculation) is an experimental procedure: add a to every variation of other populations; with each insertion, observe before-after outcome differences, $\Delta y(a)$. An unbiased effect estimate for a is an average across all observations, and constitutes a U-Statistic [17]. There are $F_{m,n} = \sum_{t=0}^m \binom{m-t}{t}$ such sequential observations⁴. $F_{m,n}$ is the number of factor fixations after a - i.e., $\binom{m-1}{1} = m-1$ to fix any second factor, then $\binom{m-2}{2}$ to fix a third, etc.

The two previous quantities, C_m and $F_{m,n}$, appear in Pascal's triangle (adjacent side and altitude), since a *single* square can be thought as two mirrored triangles, justified to the left, Fig.1(c, middle). Since the main diagonal marks a 's distinct 'times-of-insertion', the square's upper triangle contains the set of all counterfactuals with a , and the lower, without a , Fig.1(c, right). The sample enumeration rate ω , at time t , is thus defined as $\omega = \frac{F_{m,n}}{D_n}(t)$, or, the number of external observations, $F_{m,n}(t)$, per derangement, $D_n(t)$, in a sample.

³'balance' is used as in the counterfactual effect literature [25].

⁴ $\binom{m-t}{t} = 0$, when $t > m$.

We can think of each such observation as a different 'background', or external condition, under which the effect of a (or other combinations of factors) are observed. The more backgrounds under which effects and models are observed the more confidence we have in their generalizability, or, External Validity (EV). This quantity reflect the definition for populations in the last section, and was alternatively defined in [23] (*Sect. Sample Power*). Here, we relate it in further detail to Pascal's triangle and hyperbolic geometry. These connections would prove useful to describe model generalizability in spatial systems.

The growth of C_m , D_n and $F_{m,n}$ assume Pythagorean relations⁵, Fig.1(c),

$$\left(\frac{\partial C_m}{\partial D_n}\right)^{-2} + \left(\frac{\partial D_n}{\partial D_n}\right)^{-2} = \left(\frac{\partial F_{m,n}}{\partial D_n}\right)^{-2}, \quad (4a) \quad \left(\frac{\partial C_m}{\partial F_{m,n}} \text{ const.}\right)$$

$$\frac{1}{\sqrt{1 + \left(\frac{\partial D_n}{\partial C_m}\right)^2}} = \omega, \quad (4b) \quad \frac{1}{\sqrt{1 - \omega^{-2}}} = \cosh(\omega^{-1}), \quad (4c) \quad \left(\frac{\partial F_{m,n}}{\partial D_n} = \omega\right)$$

Eq.(4a) suggests the visualization of sample growth as an hyperbolae⁶ with increasing radius D_n , Fig.1(a). The figure shows the hyperbolic asymptotes $C_m = F_{m,n}$ and $C_m = -F_{m,n}$ (dashed). They represent growth with constant EV, $\partial D_n = 0$. The figure also shows the asymptotic sample (vertical black line) where exactly all observations have factor a , $F_{m,n} = 0$. **Under this condition, no estimator, algorithm, or agent is able to estimate a 's effect.** It represents the sample with minimum EV, while outward hyperbolae, samples with increasing EV. Growth in this direction follow a Fibonacci series, whose rate is the Golden number. Notice that $\frac{\partial D_n}{\partial C_m} \in [1/e, 1/2]$, as growth can range between $\frac{\partial C_m}{\partial m} = 2$, and $\frac{\partial D_n}{\partial n} = 1/e$, Fig.1(c). The first is due to $C_m = 2^m$, and the second was established by Euler [26]. The first is, in turn, associated with purely balanced or Unconfounded (CF) growth (next section), and the second with EV sample growth patterns.

⁵the equation uses the Pythagorean theorem in its reciprocal form, as it includes the triangle's altitude.

⁶the equation for a hyperbole is $\left(\frac{x}{a}\right)^2 - \left(\frac{y}{b}\right)^2 = r$, with a and b its vertices and r radius.

The golden ratio is associated, in contrast, with growth balancing these extremes, EV-CF growth, and with squares. Also associated with squares is the assumption that $\frac{\partial C_m}{\partial F_{m,n}}$ is constant across factors (i.e., hyperbolae with constant radius), Eq.(4a). It indicates that factors' diagonals are the same size, and the population structure is, overall, a 'square'.

2.3 Sample Unconfounded (CF) Growth

We say $m - 1/m$ is the 'delay' for a single counterfactual observation in a $m \times m$ square. Any population $\{a\}$ must wait $m - 1/m$ samples to complete a square row ⁷ (i.e., collect $b, c, d, \dots [m]$). We then write $m - 1/m$ for a 's balancing cycle length, and $m + 1/m$ for its growth-balance cycle length. The growth-only length is, consequently, their difference, $2/m$. We denote population sizes in each such cycle: $n_{\bar{a}}$ (balance), n (balance-growth) and n_a (growth). Across time, these quantities express the added cost populations incur to collect, together, a balanced sample. Across space, they indicate the spatial-level in which they become balanced. Population size n_t , with m factors balanced, follows the periodic difference equation $n_{t+m} = n + F_{m,t}$, or,

$$n_{t+m} = \sum_{n_t} \left[\frac{1}{n_t} \left(m + \frac{1}{m} \right) + n_t \left(m - \frac{1}{m} \right) \right], \quad \sum_{n_t} \frac{1}{n_t} \left(m + \frac{1}{m} \right) \rightarrow n, \quad \sum_{n_t} n_t \left(m - \frac{1}{m} \right) \rightarrow F_{m,t} = n_{\bar{a}},$$

(5a)
(5b)
(5c)

$$\frac{\partial n_{\bar{a}}}{\partial t} = 1.6180... (\phi), \quad (5d) \quad \frac{\partial n_a}{\partial t} = 2, \quad (5e) \quad \frac{\partial n_{\bar{a}}}{\partial n_a} = \frac{\phi}{2}, \quad (5f)$$

for a constant $m \ll n$. Eq.(5c) is an alternative expression for the Fibonacci series⁸;

⁷where 1.0 is the cost to sample a new difference, with repetition.

⁸ $F_{m,t+1} = F_{m,t-1} + F_{m,t} \times \left(m - \frac{1}{m} \right)$; $F_{m,0} = 0, F_{m,1} = 1$, see [10].

and, according to Eq.(5b), with fixed m , n is fixed per population⁹.

Let \bar{x}_0 be the set of external factors for population x_0 , $\bar{x}_0 = X - x_0$. In a random sample with a single treatment indicator a , it follows that $\mathbb{E}[\frac{\partial n_a}{\partial t} | \bar{\mathbf{x}}_0] = 2$, as, at each 2 time intervals, we are expected to rebalance (random variables are bold). It corresponds to Eq.(5a) when $m = 1$, n_{t+1} . A location with this property has one population, $\{a\}$, balanced, and common external factors, $\bar{x}_0 = X - \{a\}$. We can alternatively say that $p(a|\bar{\mathbf{x}}_0) = 0.5$, or, $a \perp (X - \{a\}) | \bar{\mathbf{x}}_0$, which are typical non-confounding conditions [25, 21]. If units in the location share the same external factors, and have the same number of members with a as without a , then expected outcome differences between them correspond to a 's effect, conditional on the common variation, $\mathbb{E}[\Delta y(a) | \mathbf{x}_0] = y(x_0 + \{a\}) - y(x_0 - \{a\})$. Learning systems and agents in such locations operate with fair estimates of a 's impact (albeit, with low EV). In a square, in contrast, **all m factors are balanced simultaneously** ($m > 1$). While single-factor balance requires a binomial series, balancing several requires Fibonacci (i.e., square altitude expansion). Each population, in this case, has asymptotic period $\mathbb{E}[\frac{\partial n_a}{\partial n_{\bar{a}}}] = \frac{2}{\phi}$ (twice the delay for each altitude). Square accumulation, furthermore, increases the EV of all its populations simultaneously [23].

2.4 Sample EV-CF Growth

Euler's required period [26] to derange one population (i.e., combination of factors) is $e = 2.7182...$ Substituting this in Eq.(5a,5b,5c), for growth with unitary sample enumeration rate,

$${}^9 \sum_{n_t} \frac{1}{n_t} \left(m + \frac{1}{m} \right) = \frac{n_t \times m}{n_t} + \frac{n_t}{n_t \times m} = m + \frac{1}{m}.$$

$$\left(e + \frac{1}{e}\right) = \frac{\cosh(1)}{2}, \quad \left(e - \frac{1}{e}\right) = \frac{\sinh(1)}{2}, \quad \tanh(n) = \frac{\sinh(n)}{\cosh(n)} = \omega^{-1}, \quad (6a)$$

$$e^{\pm \operatorname{arctanh}\left(\frac{\partial D_n}{\partial F_{m,n}}\right)} = \frac{(1 \pm \frac{\partial D_n}{\partial F_{m,n}})}{\sqrt{\left(1 - \frac{\partial D_n}{\partial F_{m,n}}\right)^2}}, \quad (6b) \quad \frac{\cosh(n)}{\partial n_a} \rightarrow 0.8090... \text{ (EV-CF)}, \quad (6c)$$

which suggests that hyperbolic functions can express enumerable permutation counts in sample balance (\sinh) and growth-balance (\cosh) cycles, as well as the growth process' chosen trade-off between the two (\tanh). The same functions appeared in Eq.(3). The equations also suggest, from de Moivre's theorem, an interpretation of hyperbolic angles as the number of growth-balance cycles a system has undergone, $[\cosh(1) + \sinh(1)]^n = \cosh(n) + \sinh(n)$, and, from Euler's equation, the rate of a single cycle without balance, $e^{-1} = \cosh(1) - \sinh(1)$. Since $\cosh(n) = (1 - \tanh^2(n))^{-\frac{1}{2}}$, Eq.(4c) suggests expressing sample enumeration rates ω in terms of $\tanh(n)$ ¹⁰, Eq.(6a). Particularly, this relates $\tanh(n)$ to the reciprocal of enumeration *rates*, or, by definition, their periods as in Eq.(3). Since $\sinh'(n) = \cosh(n)$, Eq.(5f) indicates the per-population asymptotic rate in balanced growth, Eq.(6c). The hyperbole with this relative \cosh and \sinh growth rate is indicated in Fig.1(a). Also note that Eq.(4c) coincides with Lorentz factor γ [6, 12], best known as a time correction between frames-of-reference in the physical sciences. Here, it preserves frequency relations among factors, $n_a/n_{\bar{a}}$, under changes of basis of the type $x=x_0+\{a\}$ and $x=x_0-\{a\}$. As suggested by Borel [3], it is natural to think of the transformation as a hyperbolic rotation (analogously to the typical trigonometric). We will illustrate many of these very abstract concepts in the next section, *Sect. Results*, using real-world spatial

¹⁰with $n = \operatorname{arctanh}(\omega^{-1}) = \operatorname{arctanh}(\frac{D_n}{F_{m,n}})$, which, lets n be the number of accumulated derangements per fixed $F_{m,n}$ (i.e., per square), as expected.

data.

3 Results

We will now illustrate the formulated combinatorial and statistical generalizability limits in an important real-world problem: out-of-sample prediction with samples of census individuals across increasing spatial extensions. Data used encompasses microdata of American decennial censuses from 1840 to 1940, and approximately 65 billion individual-level records. This time range corresponds to the decades of American urbanization, incited by rapid industrial growth and immigration into cities. In 1840, only 10% of the American population was urban. By 1940, it already neared 60%. We consider the economic and demographic changes as we go, spatially, from the household spatial-level, d_0 in lat-lon distances, all the way to the national level, for each studied year. We thus create samples with units at arithmetically increasing levels, $d_{t+1}=d_t+\Delta d$ (starting from d_0). We repeat this for approximately 60K American locations, x_0 . Each full spatial analysis is then reproduced independently across years (avoiding issues related to extended longitudinal data). Fig.2(b, middle) shows two locations in New York City, which share a large amount of external variation (i.e., economic and demographic variations across the rest of the country). The resulting nation-wide transversal captures combinatorial patterns of populations' differences and overlaps in samples, for all x_0 , as we increase scale. Our main goal is to illustrate how, consequently, **generalizability change across spatial-scales**, according to the stipulated model and limits, Eq.(6). We, finally, repeat previous out-of-sample prediction tasks with the current data, and with increasing spatial levels - thus adding to previous evidence presented to a combinatorial counterfactual model for sample generalizability [23] .

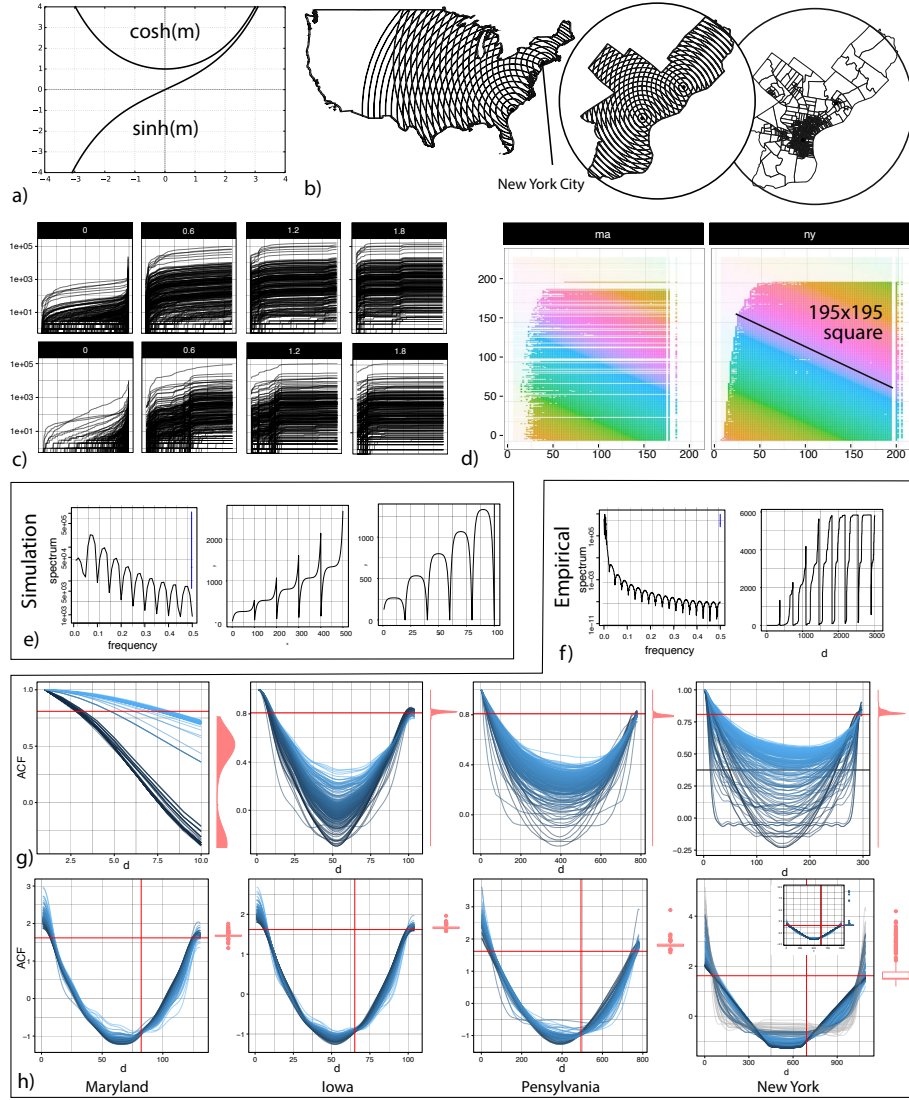


Figure 2: **(a)** sinh and cosh functions, **(b)** increasing spatial-levels at two example locations (national and city-levels), (rightmost panel) finest spatial-level for New-York City, **(c)** occupation frequency ranks vs. location across 4 example scales, each curve is an occupation, **(d)** enumerated Latin-Squares histograms for Massachusetts and New York, the latter has a square with almost all occupations, **(e)** periodogram of $\cosh(100) + \sinh(100)$, $\sinh(100)$ and $\cosh(100)$, **(f)** per-occupation periodogram and series example from (c), **(g)** auto-correlation vs. spatial-level trace catenaries (free-hanging ropes) for each occupation (1880), probability distribution of their slack (red, sidepanel) indicate a fixed cosh increase per factor at 0.81 (red horizontal line), Eq.(6c), **(h)** standardized catenaries across *all* years, boxplots (red, sidepanel) show slack invariance and constant ratio between sinh and cosh growth for all locations, years and occupations, $m \times (1 - \frac{1}{e})$ (red vertical line) is a fixed point in binomial-exponential (EV-CF) to exponential (EV) rate transitions.

3.1 Descriptive Statistics

Economic distribution across space can be described by the primary occupation and industry of all census individuals [1, 13] (e.g., 'carpenter' or 'executive assistant'). We start with this set of variables, and discuss the full set of variables, including non-economic, in the next section. Fig.2(c) illustrates empirical frequencies for all occupations (each a curve) at 4 different spatial-levels in Massachusetts (MA) and New York (NY), 1880. They were the country's economic centers until the 19th century. The distribution has the familiar shape of a wave that moves to the left. New York reaches a stationary shape at a lower level d_{sq} . We demonstrate these correspond to levels where squares are completed across factors. All squares in a location can be enumerated through an expensive computational procedure [23]. Fig.2(d) shows histograms, where each color corresponds to one of 220 occupations. NY has a spatial square that extends to almost all occupations, while MA has missing occupations (horizontal gaps) in comparison.

3.1.1 A 'Hanging-Rope' Model for Unbiased Sample Growth

The Catenary is a curve with long scientific history. Unlike circles and geodesics, they are sums of exponentials. Catenaries describe a free-hanging rope, whose 'slack' h is the difference in height, y , between its two hanging points [7]. Their equation in (x, y) Cartesian coordinates is $y = h \cosh(\frac{x}{h})$, and their length is $h \sinh(\frac{x}{h})$, making them useful to demonstrate the previous model, Eq.(6), and increases in enumerable permutations across spatial levels. We demonstrate that both the empirical shape, Fig.2(h), and slack parameter, Fig.2(h, boxplots), of spatial correlations follow predictions from the previous model. Before considering catenaries, however, Fig.2(a,e) illustrate the overall shape of the previous hyperbolic functions, and their frequency-based representations. Fig.2(a) de-

picts $\cosh(n)$ and $\sinh(n)$, and, Fig.2(e) the periodogram of $\cosh(n)+\sinh(n)$, $\sinh(n)$ and $\cosh(n)$ where $n = 100$. Fig.2(f) illustrates the *empirical* periodogram of curves in Fig.2(c), which resemble the simulated.

Fig.2(g) shows auto-correlations (ACF) for all locations across 5K spatial-levels (as those illustrated in Fig.2(c)), until the state level. They trace catenaries. The horizontal line $y = 1.0$, of unitary correlation, is associated with the limit $F_{m,n} = 0$ where, despite the increasing scale, no population differences are added to the increasing samples. Each single catenary is a set of samples with constant $C_m/F_{m,n}$, which is a **defining property of squares**, Eq.(4a). Fig.2(g) illustrates 4 typical cases among states. Plots for all states are available in the Supplementary Material. Maryland has linear decreases in auto-correlation. From 1840, the USA economy and cities become increasingly interdependent. After 1900, no longer any state had such linear correlation signatures. Periodic and linear (zig-zag) auto-correlations, with period $m/2$, are related to non-increasing EV, Fig.1(a, black vertical line). Periodic and exponential correlations, without growth, correspond to catenaries with $h = 0$ (where a system returns to its original state after a lag). Standardizing catenaries make h indicate relative growth rate [7], $h = \cosh(m) - \cosh(0)$.

Fig.2(h) shows standardized catenaries for all years and locations. It indicates that \cosh per factor remains constant across a range of levels, up to d_{sq} , starting at the local. This was anticipated by Eq.(6c). The rate, up to d_{sq} , is 81% of correlation. Fig.2(h, sidepanel, red) shows **box-plots** for h , across all levels, years, occupations, and locations. For all spatial-levels below d_{sq} , factors a and \bar{a} remain balanced, with binary-exponential rates (i.e., hyperbolic functions with period $m/2$). Levels above d_{sq} reverse to exponential growth. We called this a transition between EV-CF and EV growth. This is indicated in plots by the dislocation of the catenary center from $m/2$ to $m(1-1/e)$ (red vertical lines). We reproduce

the same results, Fig.2(g,h), with standard **Pareto regressions** in *Sect. Methods* of the *Supplementary Material* - as alternative to these graphical depictions. Fig.3(d) shows estimated levels d_{sq} for all states, across years. Levels d_{sq} converge across years for all states. New York has 2-level squares. Fig.2(h, upright-panel) shows catenaries for its lower-level square, and Fig.3(b) illustrate levels cartographically. The two squares' factors are disjoint (gray, lower factors taking exponential rates in higher). American states have had through their histories very different work forces and regional distributions. While catenary lengths are different across occupations, Fig.2(g), their slack (and cosh-sinh growth ratio) **remains invariant across all locations, years and occupations**, Fig.2(h). These considerations will be key to solving our main problem, Eq.(1), as the accuracy of agents and algorithms operating in samples with these combinatorial patterns are directly determined by sample factor correlations [23]. These plots will thus graphically illustrate combinatorial constraints for the unbiasedness and predictiveness of learning systems across space. We return to this discussion in *Sect. Predictive Statistics*.

3.1.2 Permutations in Heterogeneous Samples

Zipf's law and distribution are central to the study of city size distributions [19, 9, 2]. The law is based on a frequency ranking of studied factors, and thus, on one of their permutations. It is, here, associated with homogeneous samples (i.e., samples with little variation). Fig.3(a) depicts the overall shapes of $\tanh(n)$ and $\coth(n)$ functions. Fig.3(h) shows occupations' minimum frequency rank, r_0 (green), across all locations in increasing spatial levels, as well as their maximum rank, r_ω (red). The former is the minimum frequency ranking order of one given occupation across all of the level's locations. The latter is the maximum (these are formulated explicitly in *Sect. Methods*). The latter is related to Zipf's frequency rankings and the Pareto distribution (*Sect. Methods*), as the three

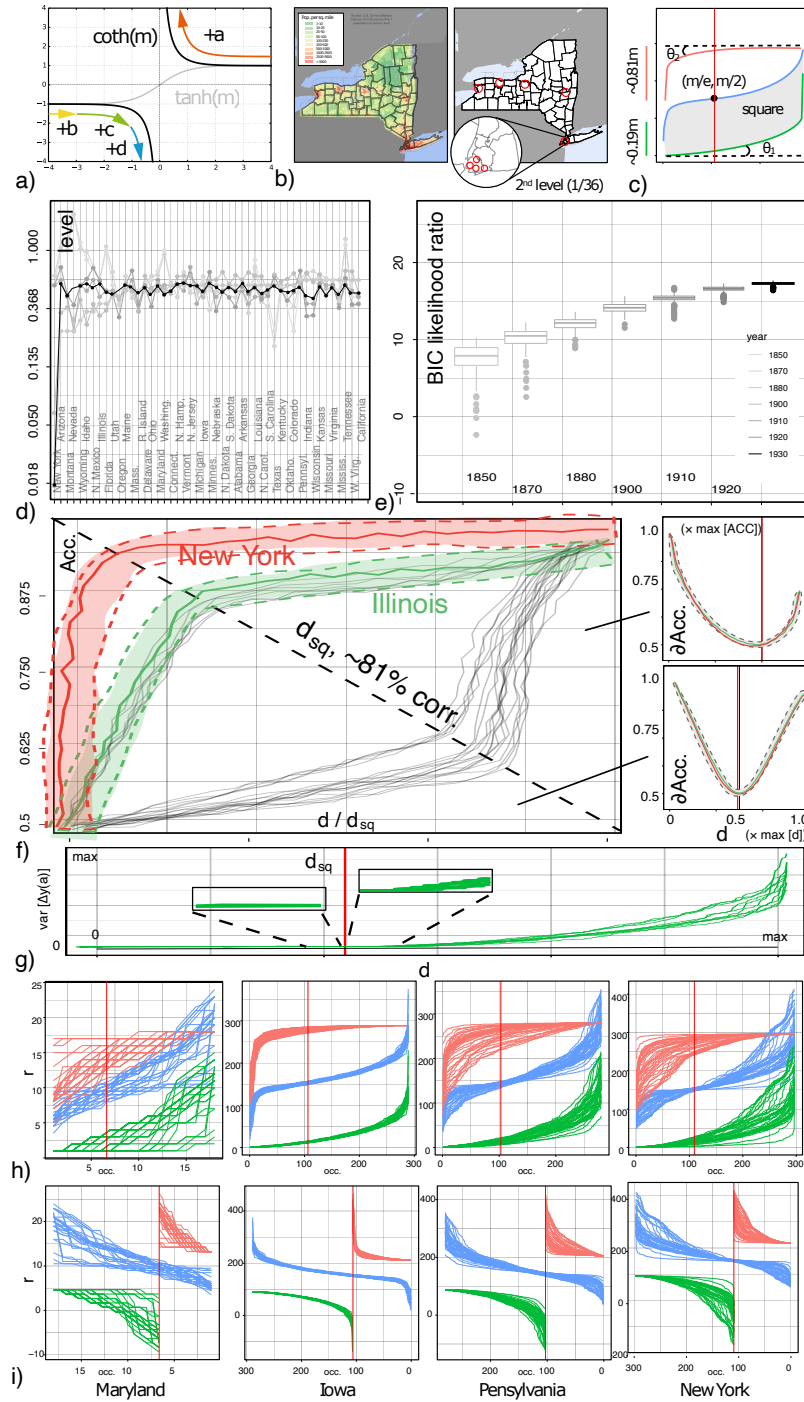


Figure 3: (a) \coth and \tanh functions, colored arrows illustrate square factor frequency increases with scale, (b) New York (NY) state population density (left), NY has squares at two levels d_{sq} , at 0.018 and 0.65 lat-lon distances (red circles), (c) schematic depiction of frequency rank vs. spatial-scale plots in (h), (d) d_{sq} (spatial-level of first square) for states and years, (e) BIC likelihood of coth over a Zipf model, (f) state-of-the-art growth prediction's accuracy with increasing spatial-level d , d_{sq} is diagonal (dashed), (g) min. (green) and max. (red) frequency ranks across locations, each curve is a scale, blue curves indicate square size, which follows a tanh function, (h) coth model, as illustrated in (a), with empirical data.

are Power-laws. Each curve in the figure corresponds to one spatial-level and occupation. With a homogeneous sample, we expect one highest-rank industry across all locations, and thus $r_\omega - r_0 = 1$. What we observe, however, is that factors are ranked in constant-sized ranges, as visualized in squares. Each factor is the highest ranked in *some* location, the second in other, etc. These rankings define an arithmetic series $-r_0, r_0 + 1, r_0 + 2, \dots, r_\omega -$ for each factor. The series has mean $\bar{r} = \frac{r_0 + r_\omega}{2}$, which is also shown (blue). The previous model predicts both that $r_\omega - r_0$ is constant, and that it reflects the enumeration rate ω . Fig.3(h) shows that empirical rankings have constant $r_\omega - r_0$, with increasing r_0 . A closer examination of both branches (red and green) reveals they correspond to the positive and negative sections of the $\coth(n) = 1/\tanh(n)$ function, Fig.3(i,a).

Imagine the following process: pick a location x_0 , and its most and least-frequent factors (i.e., with rank 1 and m). Label them, respectively, a and z . Balance z to match a 's frequency. Move one spatial-level up, pick another z , balance, and repeat. In a square row, n_a is the number of units in cell a , and $n_{\bar{a}}$ in other cells (i.e., not a). The cost to balance each z is thus n_a/ω . For all locations x_0 , and levels $d_0 \leq d \leq d_{sq}$,

$$\begin{aligned} n_a \times \frac{1}{\omega} - n_{z \in \bar{a}} &= 0, \\ n_a - n_{z \in \bar{a}} \times \coth(n) &= 0, \end{aligned} \tag{7}$$

which implies $\sum_{i=0}^{sq} n_{z_i} = n_{\bar{a}}$, and $n_a = n_{\bar{a}}$. The \coth function separates, by sign, each location's balancing and growth phases, and reveals how (order, magnitude) squares are completed, Fig.3(a). This is illustrated as one hyperbolic rotation, with subsequent square derangements leading to others.

Methodologically, this suggests fitting a \coth function to observed frequency ranks. A

Zipf-distribution can be fit by Power-law or Pareto distribution regressions (*Sect. Methods*). Enumeration rate increases imply increasing permutations - and thus differences between min. and max-frequency ranks. This predicts that Zipf-Pareto regressions will become increasingly inaccurate (compared to coth), as cities become more heterogeneous. Fig.3(e) shows increase of up to 18 times fit likelihood favoring the coth model throughout the studied period, according to a Bayesian Information Criterion.

3.2 Predictive Statistics (Reproduction of [23])

What impact does the presence of squares have in samples statistically (in respect to bounds to their predictiveness and biasedness)? This was formulated theoretically, and demonstrated practically in simulated, cohort, experimental, economic, and genetic data [23, 22]. Fig.3(f) demonstrates a further result, using census microdata, with an Accuracy vs. Spatial-level plot. Samples in the previous section contained sample units' primary occupations [4, 20]. This led to binary samples of dimension $m = 543$ (and, each unit seen as a 543 length binary vector). For Fig.3(f), all variables in the American micro census were, instead, used [14]. Each census binary variable lead to one field, each categorical variable to as many binary variables as the size of their domain (as defined by the census) and continuous variables to 8-bit vectors (corresponding to their 8 quantiles). The final sample had 10.055 variables, including information on a broad range of population characteristics, including fertility, nuptiality, life-course transitions, immigration, internal migration, labor-force participation, occupational structure, education, ethnicity, and household composition. These variables can be correlated, colinear and spurious. Each of the multiple state-of-the-art classifiers employed next will deal with these statistical pitfalls in their own proposed ways.

The classification task in Fig.3(f) is to predict whether a given occupation will grow (enlist further members) in the next time interval (10 years ahead), for each location x_0 . Detailed description of algorithms used, and their hyperparameter optimization, can be found on [23]. They include Neural Network Models, Generalized Linear Models, Boosting Models, Generalized Additive Models, Random Trees, LASSO and Ridge regressions, ANOVA, Support Vector Machine, and stacked meta-learners for all previous algorithms. Spatial levels (and aggregated data) ranged from the local to the national. One million location and year pairs were chosen randomly, each leading to a full set of spatially growing samples. The figure thus shows the maximum accuracy of 24 state-of-the-art supervised algorithms, to predict whether a given occupation will grow, or not, in a location, as we use data from increasing spatial-levels (starting with the local and reaching all national). Accuracy is defined as the number of accurately classified observations in the held-out sampled. Spatial levels d_{sq} for each state are mapped to the diagonal (dashed) in the figure, and each state is a curve. Accuracy was averaged across same-state locations to generate these curves. Bootstrap accuracy variation bands (across states' locations) are shown for the two most accurate states, New York and Illinois. We observe that New York gains little from external data, above d_{sq} , as it already contains, within its boundaries, high levels of variation. This also implies that, without unobservables, $\sim 81\%$ of the sample is sufficient for prediction. Homogeneous locations, in contrast, have **incomplete squares**, and observed predictions are susceptible to external and unobserved variation [23].

The right panels in Fig.3(f) shows the *increase* in accuracy, $\partial ACC/\partial d$, of systems with increasing distances (at 0.05 lat-lon intervals, normalized over their spatial and accuracy ranges) for New York and Illinois. This is the difference in accuracy of models trained at a level d and its predecessor. The top panel shows accuracy of algorithms with samples

with observations $d > d_{sq}$, and bottom panel $d \leq d_{sq}$, across all locations in those states (gray ribbons show their standard deviation). These patterned differences in accuracy changes, in the output of supervised black-box algorithms, mirror the shape of functions in Fig.2(g,h). This is expected as the accuracy of systems with characteristics described above increase with pairwise correlations [23]. The functional form for accuracy $\mathcal{F}(d, \mu) = \mu \times \sinh(d)$ take, therefore, hyperbolic forms with distinct parameters, $\mu = 0.5 \times m$ and $\mu = (1 - 1/e) \times m$, and constant tanh, $0 \leq \mathcal{F}(d, \mu) \leq 1$. The 80-20 ratios, observed for correlations in *Sect. A 'Hanging-Rope' Model for Unbiased Sample Growth*, are thus also observed in the outcome of black-box predictors, Fig.3(f). Like before, the functional $\mathcal{F}(d, \mu)$ is an apt description in these systems only because tanh also remain constant throughout them (i.e., in squares and balanced samples), Eq.(4a).

Given the balance of samples in $d < d_{sq}$, it is expected for effect estimation to become easier in these samples, in contrast to samples $d > d_{sq}$. In [23], we use multiple simulated scenarios to show that samples with the combinatorial conditions like those in $d < d_{sq}$ facilitate causal effect estimation. This is possible because, there, we have groundtruth information for the effect of variables. We do not have groundth in this large real-world system, but the central claim here is that in $d > d_{sq}$ samples the problem becomes harder. Fig.3(g) shows variance in effect estimation for the popular Shapley-based effect estimation [18] across all locations x_0 and distances d , and the previous samples. There is a discontinuity, and significant increase in uncertainty over effect estimates above d_{sq} (and very little below), across all locations. Together, the previous considerations suggest constraints, described by $\mathcal{F}(d, \mu)$, for supervised prediction and effect estimation in spatial systems. Functions $\mathcal{F}(d, (1-1/e)m)$ and $\mathcal{F}(d, 0.5m)$ describe, respectively, patterns of externally-valid (EV) and unconfounded (EV-CF) spatial sample growth.

4 Conclusion

We studied applications of concepts from non-parametric and counterfactual statistics to sample growth processes; common, for example, in the study of spatial systems. We highlighted samples where m populations can remain unbiased, with increasing generalizability. The set of all squares of size m is related both to an optimal estimator in Theoretical Statistics and a solution in Cooperative Game-Theory. Hyperbolic functions offered a natural implementation and visualization for these alternative growth patterns. Increase in generalizability, for $m = 1$, requires exponential sample size growth. Increase in unbiasedness requires Fibonaccian, with a half-golden growth ratio. We demonstrated the model empirically (functional-form, enumerative and combinatorial properties, 3 predicted rates), and connected growth to the statistical environment (biases and predictability) it creates for populations.

Declarations

Conflicts of interest/Competing interests: No conflicts to declare.

Availability of data and material: The datasets analysed in the current study are available in the IPUMS repository [14].

Funding: Funding provided by the Sao Paulo Research Foundation (FAPESP).

Authors' contributions: AFR is the sole author.

References

- [1] Pierre Alexane Balland, Cristian Jara-Figueroa, Sergio G Petralia, Mathieu P. A Steijn, David L Rigby, and César A Hidalgo. Complex economic activities concentrate in large cities. *Nature human behaviour*, 4(3):248–254, 2020. doi: 10.1038/s41562-019-0803-3.
- [2] Marcus Berliant and Axel H. Watanabe. A scale-free transportation network explains the city-size distribution. *Quantitative Economics*, 9(3):1419–1451, 2022/05/30 2018. doi: <https://doi.org/10.3982/QE619>. URL <https://doi.org/10.3982/QE619>.
- [3] Emile Borel. *Introduction geometrique a quelques theories physiques*. Paris, 1914.
- [4] Census Bureau. *Alphabetical index of industries and occupations. 1950 census of population*. Washington, 1951.
- [5] Nadia Burkart and Marco F. Huber. A survey on the explainability of supervised machine learning. *J. Artif. Int. Res.*, 70:245–317, may 2021. ISSN 1076-9757. doi: 10.1613/jair.1.12228. URL <https://doi.org/10.1613/jair.1.12228>.
- [6] Sean Carroll. *Spacetime and Geometry: An Introduction to General Relativity*. Benjamin Cummings, 2003. ISBN 0805387323.
- [7] Paul Cella. Reexamining the catenary. *The College mathematics journal*, 30(5):391–393, 1999. doi: 10.1080/07468342.1999.11974093.
- [8] Paul de Boer and João F. D Rodrigues. Decomposition analysis: when to use which method? *Economic systems research*, 32(1):1–28, 2020. doi: 10.1080/09535314.2019.1652571.

- [9] X Gabaix. Zipf’s law for cities: An explanation. *The Quarterly journal of economics*, 114(3):739–767, 1999. doi: 10.1162/003355399556133.
- [10] Midhat J Gazale. *Gnomon: from pharaohs to fractals*. Princeton University Press, Princeton, N.J, 1999. ISBN 0691005141; 9780691005140.
- [11] Wassily Hoeffding. A class of statistics with asymptotically normal distribution. *The Annals of mathematical statistics*, 19(3):293–325, 1948. doi: 10.1214/aoms/1177730196.
- [12] Joseph Hucks. Hyperbolic complex structures in physics. *Journal of mathematical physics*, 34(12):5986–6008, 1993. doi: 10.1063/1.530244.
- [13] Hong Inho, Frank Morgan R., Rahwan Iyad, Jung Woo-Sung, and Youn Hyejin. The universal pathway to innovative urban economies. *Science Advances*, 6(34):eaba4934, 2022/06/18. doi: 10.1126/sciadv.aba4934. URL <https://doi.org/10.1126/sciadv.aba4934>.
- [14] IPUMS. U.s. individual-level census (united states bureau of the census), 2022. URL https://usa.ipums.org/usa/complete_count.shtml.
- [15] Jon Kleinberg, Jens Ludwig, Sendhil Mullainathan, and Ziad Obermeyer. Prediction policy problems. *The American economic review*, 105(5):491–495, 2015. doi: 10.1257/aer.p20151023.
- [16] Christopher Krapu, Robert Stewart, and Amy Rose. A review of bayesian networks for spatial data. *ACM Trans. Spatial Algorithms Syst.*, mar 2022. ISSN 2374-0353. doi: 10.1145/3516523. URL <https://doi.org/10.1145/3516523>. Just Accepted.

- [17] A. J. Lee. *U-statistics : theory and practice*. M. Dekker, New York, 1990. ISBN 0824782534.
- [18] Scott M. Lundberg and Su-In Lee. A unified approach to interpreting model predictions. In *Proceedings of the 31st International Conference on Neural Information Processing Systems*, NIPS’17, pages 4768–4777, Red Hook, NY, USA, 2017. Curran Associates Inc. ISBN 9781510860964.
- [19] MEJ Newman. Power laws, pareto distributions and zipf’s law. *Contemporary Physics*, 46(5):323–351, 09 2005. doi: 10.1080/00107510500052444.
- [20] Anastasiya M Osborne, United States. Bureau of Labor Statistics. Office of Productivity, Technology, and Peter B Meyer. *Proposed category system for 1960-2000 census occupations*. U.S. Dept. of Labor, Bureau of Labor Statistics, Office of Productivity and Technology, Washington, D.C.], 2005.
- [21] Hans Reichenbach. *The direction of time*,. University of California Press, Berkeley, 1956.
- [22] Andre F. Ribeiro. Population structure and effect generalization, 2022. URL <https://arxiv.org/abs/2209.13560>.
- [23] Andre F. Ribeiro. The external validity of combinatorial samples and populations, 2022, Under Review. URL <https://arxiv.org/abs/2108.04376>.
- [24] Alvin E. Roth. *The Shapley Value: Essays in Honor of Lloyd S. Shapley*. Cambridge University Press, Cambridge, 1988. ISBN 9780521361774. doi: DOI:10.1017/CBO9780511528446. URL <https://www.cambridge.org/core/books/shapley-value/D3829B63B5C3108EFB62C4009E2B966E>.

- [25] Donald B Rubin. Causal inference using potential outcomes: Design, modeling, decisions. *Journal of the American Statistical Association*, 100(469):322–331, 2005. doi: 10.1198/016214504000001880.
- [26] Charles Edward Sandifer. *How Euler did it (Chapter 17, pg.103)*. The MAA tercentenary Euler celebration ; v.3. Mathematical Association of America, Washington, DC], 2007. ISBN 9780883855638.
- [27] Shashi Shekhar. What is special about spatial data science and geo-ai? In *33rd International Conference on Scientific and Statistical Database Management, SSDBM 2021*, page 271, New York, NY, USA, 2021. Association for Computing Machinery. ISBN 9781450384131. doi: 10.1145/3468791.3472263. URL <https://doi.org/10.1145/3468791.3472263>.
- [28] Shashi Shekhar and Pamela Vold. *MIT Press Essential Knowledge series*. The MIT Press, Cambridge, 2020. ISBN 0-262-35681-3.
- [29] Ilaria Tiddi and Stefan Schlobach. Knowledge graphs as tools for explainable machine learning: A survey. *Artificial Intelligence*, 302:103627, 2022. doi: <https://doi.org/10.1016/j.artint.2021.103627>. URL <https://www.sciencedirect.com/science/article/pii/S0004370221001788>.
- [30] Hajime Yamato and Yoshihiko Maesono. Invariant u-statistics. *Communications in statistics. Theory and methods*, 15(11):3253–3263, 1986. doi: 10.1080/03610928608829307.